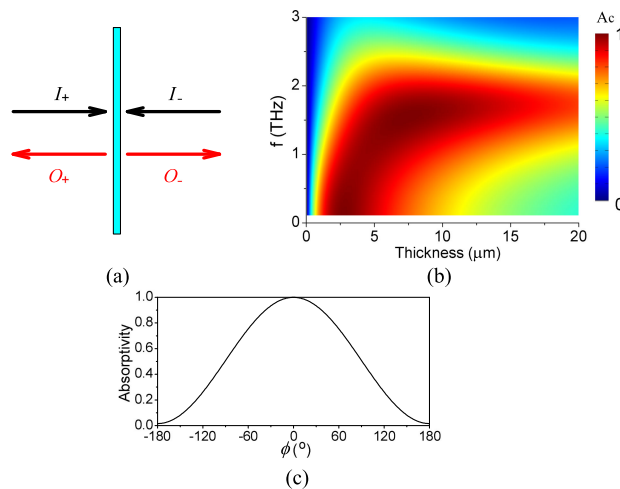


# MoS<sub>2</sub> Broadband Coherent Perfect Absorber for Terahertz Waves

Volume 8, Number 6, December 2016

Weiren Zhu  
Fajun Xiao  
Ming Kang  
Debabrata Sikdar  
Xianling Liang  
Junping Geng  
Malin Premaratne  
Ronghong Jin



---

DOI: 10.1109/JPHOT.2016.2633571  
1943-0655 © 2016 IEEE

# MoS<sub>2</sub> Broadband Coherent Perfect Absorber for Terahertz Waves

Weiren Zhu,<sup>1</sup> Fajun Xiao,<sup>2</sup> Ming Kang,<sup>3</sup> Debabrata Sikdar,<sup>4</sup>  
 Xianling Liang,<sup>1</sup> Junping Geng,<sup>1</sup> Malin Premaratne,<sup>5</sup>  
 and Ronghong Jin<sup>1</sup>

<sup>1</sup>Department of Electronic Engineering, Shanghai Jiao Tong University,  
 Shanghai 200240, China

<sup>2</sup>Key Laboratory of Space Applied Physics and Chemistry, Ministry of Education, and  
 Shaanxi Key Laboratory of Optical Information Technology, School of Science,  
 Northwestern Polytechnical University, Xi'an 710129, China

<sup>3</sup>College of Physics and Materials Science, Tianjin Normal University, Tianjin 300387, China

<sup>4</sup>Department of Chemistry, Faculty of Natural Sciences, Imperial College London, London  
 SW7 2AZ, U.K.

<sup>5</sup>Advanced Computing and Simulation Laboratory, Department of Electrical and Computer  
 Systems Engineering, Monash University, Clayton, Vic. 3800, Australia

DOI:10.1109/JPHOT.2016.2633571

1943-0655 © 2016 IEEE. Translations and content mining are permitted for academic research only.

Personal use is also permitted, but republication/redistribution requires IEEE permission.

See [http://www.ieee.org/publications\\_standards/publications/rights/index.html](http://www.ieee.org/publications_standards/publications/rights/index.html) for more information.

Manuscript received September 27, 2016; accepted November 25, 2016. Date of publication December 1, 2016; date of current version December 15, 2016. This work was supported in part by the National Natural Science Foundation of China under Grant 61201058, Grant 61308031, Grant 11304226, Grant 61571298, and Grant 61571289; in part by the Fundamental Research Funds for the Central Universities under Grant 3102015ZY062; and in part by the Australian Research Council under Grant DP140100883. Corresponding authors: W. Zhu and F. Xiao (e-mail: weiren.zhu@sjtu.edu.cn; fjxiao@nwpu.edu.cn).

**Abstract:** We present a comprehensive analysis of terahertz waves propagation through a bulk MoS<sub>2</sub> crystal slab. It is shown that broadband coherent perfect absorption can be achieved and the coherent absorptivity can be adjusted from 1.57% to 99.97% by means of phase modulation. Moreover, the relative bandwidth for over 90% coherent absorptivity can be as wide as 179%. By increasing the doping rate in MoS<sub>2</sub> crystal, the coherent absorptivity spectrum exhibits a clear blueshift whilst the peak coherent absorptivity remains over 99.9%. Full-wave numerical simulations are further carried out to confirm the validity of our theoretical analysis.

**Index Terms:** Coherent perfect absorber, broadband, MoS<sub>2</sub>.

## 1. Introduction

As a contender of graphene, molybdenum disulfide (MoS<sub>2</sub>) has attracted immense popularity owing to its distinctive physical, electronic, and optical properties [1]–[4]. The bulk MoS<sub>2</sub> crystal is an indirect bandgap semiconductor with a large bandgap energy (around 1.3 eV), while it can be transformed into a direct semiconductor in the monolayer limit [5]. Therefore, MoS<sub>2</sub> shows more favourable electronic properties than those of graphene for design of next generation electronic devices. In particular, Jayasekara *et al.* [6] presented a spaser made of a circular shaped highly doped MoS<sub>2</sub> resonator which has lower operating threshold and higher mode energy than graphene based spasers. Deng *et al.* [7] found that the total losses due to the reflection and absorption of a monolayer MoS<sub>2</sub> is three orders lower than those of graphene.

On another hand, with the development of metamaterials and metasurfaces, there is an enormous interest in perfect absorption [8]–[11]. Metamaterial absorbers with subwavelength thickness and nearly perfect absorption have been widely investigated for applications such as light harvesting [12], biomedical sensing [13], and electromagnetic shielding [14]. Recently, considerable research effort has been spent on realizing perfect absorption in a system where two coherent beams incident from opposite sides onto an absorbing medium. The coherent perfect absorption can be achieved by utilizing destructive interference of reflected and transmitted waves resulting from incident beams at both sides. This scheme is widely referred as coherent perfect absorption (CPA) [15]–[17]. Unlike metamaterial absorbers whose absorptivities are fixed to the initial design, the absorptivity in a coherent system can be flexibly controlled through phase modulation of the two coherent incident waves [18], [19], which are very attractive for applications including transducers, modulators, and electromagnetic switchers.

As a time-reversed analog of lasing, CPA is commonly achieved using a metasurface composed of complicated subwavelength resonators and thus has a narrow bandwidth, which prevents it from being used in broadband applications [20], [21]. In this paper, we theoretically demonstrate that broadband CPA can be achieved in a bulk MoS<sub>2</sub> crystal. The reflection and transmission coefficients of an electromagnetic wave propagating through an MoS<sub>2</sub> crystal are analysed by characterizing MoS<sub>2</sub> crystal's dispersive permittivity using Drude's model and enforcing the boundary conditions at both surfaces of the MoS<sub>2</sub> slab. It is shown that the electromagnetic energy of two anti-propagating waves from both sides of the MoS<sub>2</sub> slab can be almost totally absorbed and the coherent absorptivity can be adjusted effortlessly from nearly 0 to 100% by phase modulation. It is also demonstrated that the absorptivity spectrum of the MoS<sub>2</sub> crystal can be controlled by electrochemical doping. As we increase the doping rate, the spectrum of coherent absorptivity exhibits a clear blueshift whilst the peak coherent absorptivity stays nearly uniform. Furthermore, full-wave numerical simulations are carried out for the purpose of verifying the accuracy of our theoretical estimates.

## 2. Theoretical Analysis

A bulk MoS<sub>2</sub> crystal can be considered as the layer-by-layer stack of MoS<sub>2</sub> monolayers bounded by weak van der Waals forces, where strong interactions only exist within the basal plane of covalent bonds. Therefore, MoS<sub>2</sub> crystal is highly anisotropic, which can be characterized with an anisotropic dielectric permittivity having an in-plane term  $\varepsilon_{\parallel}$  and an out-of-plane term  $\varepsilon_{\perp}$  [22]. The out-of-plane term is chosen to be  $\varepsilon_{\perp} = 7.43$ , which is obtained from *ab initio* calculations [23]. The in-plane term of the effective relative dielectric permittivity of MoS<sub>2</sub> crystal at terahertz (THz) frequencies follows the Drude model [24], [25]

$$\varepsilon_{\parallel} = \varepsilon_{\infty} + \frac{\omega_p^2}{\omega^2 - i\Gamma\omega}, \quad (1)$$

where  $\varepsilon_{\infty} = 11.475$  is the dielectric constant at high frequency limit,  $\omega_p = \sqrt{Ne^2/(\varepsilon_0 m^*)}$  is the plasma frequency, and  $\Gamma = e/(m^* \mu_c)$  is the damping rate of the carriers. Here,  $e$  is the charge of an electron,  $m^* = 0.58m_e$  is the effective mass of the carriers with  $m_e$  being the mass of an electron,  $\mu_c$  is the carrier mobility, and  $N$  is the intrinsic carrier density. We assume  $\Gamma/2\pi = 1.17$  THz, which was retrieved from experimental data [24], and the plasma frequency  $\omega_p$  can be adjusted by controlling the carrier density in MoS<sub>2</sub> crystal via electrochemical doping. In Fig. 1, we show the effective dielectric permittivity of MoS<sub>2</sub> crystal with different carrier densities. It is seen that when increasing  $N$  from  $5 \times 10^{16} \text{ cm}^{-3}$  to  $5 \times 10^{17} \text{ cm}^{-3}$ , the real component of  $\varepsilon_{\parallel}$  decreases from positive to negative, exhibiting the transition of MoS<sub>2</sub> crystal from dielectric to metallic phase. On the other hand, the imaginary component of  $\varepsilon_{\parallel}$  increases significantly. It is worth noting that, for each case, the imaginary component is much higher than the real component, which can be attributed to the relatively high damping rate.

Fig. 2 shows schematically an electromagnetic wave propagating upon an MoS<sub>2</sub> crystal slab placed at  $0 \leq x \leq d$ . We start our analysis by considering a *y*-polarized wave propagating from left

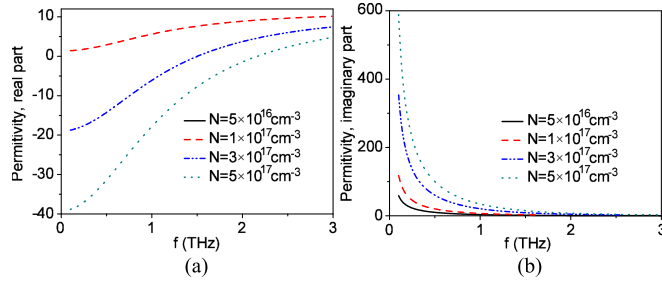
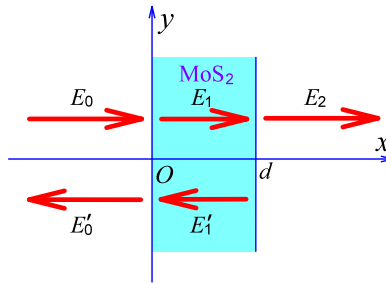


Fig. 1. In-plane component of MoS<sub>2</sub> crystal's effective permittivities with different carrier densities. (a) Real components and (b) imaginary components.



to right  $\vec{E}_0 = \hat{y}E_0 \exp[i(k_0x - \omega t)]$ , where  $\hat{y}$  is the unit polarization vector along the  $y$  direction,  $\omega$  is the angular frequency, and  $k_0 = \omega/c$  is the wave vector in free space. For sake of simplicity, we will omit the time variation  $\exp(-i\omega t)$  in the following analysis.

The electromagnetic fields in the left region can be represented as a superposition of forward and backward propagating waves

$$\vec{E}_L = \hat{y}(E_0 e^{ik_0 x} + E'_0 e^{-ik_0 x}) \quad (2a)$$

$$\vec{H}_L = \frac{\hat{z}}{Z_0}(E_0 e^{ik_0 x} - E'_0 e^{-ik_0 x}) \quad (2b)$$

where  $\hat{z}$  is the unit polarization vector along the  $z$  direction, and  $Z_0 = \sqrt{\mu_0/\epsilon_0}$  is the free space impedance. Similarly, electromagnetic fields inside the MoS<sub>2</sub> crystal slab also have forward and backward terms

$$\vec{E}_{\text{MoS}_2} = \hat{y}(E_1 e^{ik_1 x} + E'_1 e^{-ik_1 x}) \quad (3a)$$

$$\vec{H}_{\text{MoS}_2} = \frac{\hat{z}}{Z_1}(E_1 e^{ik_1 x} - E'_1 e^{-ik_1 x}) \quad (3b)$$

where  $Z_1 = \sqrt{\mu_0/(\epsilon_0 \epsilon_{||})}$ , and  $k_1 = k_0 \sqrt{\epsilon_{||}}$  are the impedance of and the wavenumber inside the MoS<sub>2</sub> crystal slab, respectively. We assume the right region in Fig. 2 is a semi-infinite open space where no reflection occurs. Therefore, the electromagnetic field in the right region has only a forward term

$$\vec{E}_R = \hat{y}E_2 e^{ik_0(x-d)} \quad (4a)$$

$$\vec{H}_R = \frac{\hat{z}}{Z_0} H_2 e^{ik_0(x-d)}. \quad (4b)$$

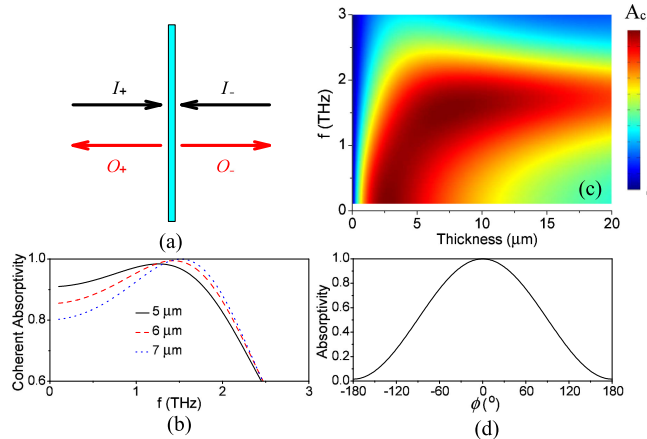


Fig. 3. (a) Coherent interaction of electromagnetic wave with subwavelength MoS<sub>2</sub> crystal layer. (b) Coherent absorptivity of MoS<sub>2</sub> crystal slab ( $N = 3 \times 10^{17} \text{ cm}^{-3}$ ) as a function of frequency and thickness. (c) Coherent absorptivity spectra of MoS<sub>2</sub> crystal slabs at three representative thicknesses of 5, 6, and 7  $\mu\text{m}$ . (d) Coherent control of the total absorptivity by phase modulation.

Continuity of electric and magnetic fields at the boundaries  $x = 0$  and  $x = d$  yields to

$$E_0 + E'_0 = E_1 + E'_1 \quad (5a)$$

$$\frac{1}{Z_0}(E_0 - E'_0) = \frac{1}{Z_1}(E_1 - E'_1) \quad (5b)$$

$$E_1 e^{ik_1 d} + E'_1 e^{-ik_1 d} = E_2 \quad (5c)$$

$$\frac{1}{Z_1}(E_1 e^{ik_1 d} - E'_1 e^{-ik_1 d}) = \frac{E_2}{Z_0}. \quad (5d)$$

By solving (5), the complex reflection and transmission coefficients of the MoS<sub>2</sub> crystal slab are obtained.

$$r = \frac{E'_0}{E_0} = \frac{1 + M - (1 - M)\sqrt{\varepsilon_{||}}}{1 + M + (1 - M)\sqrt{\varepsilon_{||}}} \quad (6a)$$

$$t = \frac{E_2}{E_0} = \left(1 + r - \frac{2r}{1 + \sqrt{\varepsilon_{||}}}\right) e^{ik_1 d} \quad (6b)$$

where

$$M = \frac{\sqrt{\varepsilon_{||}} - 1}{\sqrt{\varepsilon_{||}} + 1} e^{j2k_1 d}.$$

We now consider the interaction of two anti-propagating electromagnetic waves with a subwavelength MoS<sub>2</sub> slab shown schematically in Fig. 3(a). In such a system, the forward and backward scattering electromagnetic fields ( $O_{\pm}$ ) and the two input fields ( $I_{\pm}$ ) can be connected through a scattering matrix  $S$

$$\begin{pmatrix} O_+ \\ O_- \end{pmatrix} = S \begin{pmatrix} I_+ \\ I_- \end{pmatrix} \triangleq \begin{pmatrix} r & t \\ t & r \end{pmatrix} \begin{pmatrix} I_+ \\ I_- \end{pmatrix}. \quad (7)$$

The scattering matrix has a symmetric eigenvector  $[1, 1]^T$  and an antisymmetric eigenvector  $[1, -1]^T$ . For an MoS<sub>2</sub> layer with thickness much smaller than the operating wavelength, the anti-symmetric eigenvector  $[1, -1]^T$  has an eigenvalue  $-1$ , corresponding to the plane of the MoS<sub>2</sub> at a standing wave's node where electromagnetic losses vanish. Therefore, CPA can occur only for

the case of symmetric incidence, corresponding to  $I_+ = I_-$ , where the coherent absorptivity can be expressed as

$$A_c = 1 - \frac{|Q_+|^2 + |Q_-|^2}{|I_+|^2 + |I_-|^2} = 1 - |r + t|^2. \quad (8)$$

### 3. Results and Discussion

To investigate the terahertz coherent absorption characteristics in a thin layer made of MoS<sub>2</sub> crystal, we calculate the coherent absorptivity using Eq. (8). As an example, we plot the coherent absorptivity in Fig. 3(b) for the MoS<sub>2</sub> crystal with  $N = 3 \times 10^{17} \text{ cm}^{-3}$ , illustrating the detailed dependence on the frequency and thickness of the MoS<sub>2</sub> crystal layer. It is seen that, despite the subwavelength thickness, the MoS<sub>2</sub> crystal layer shows reasonably broadband high coherent absorptivities in both frequency and thickness regimes. In particular, the coherent absorptivity in the MoS<sub>2</sub> crystal of  $5 \mu\text{m}$  thick remains higher than 90% in the wide frequency band from 0.1 to 1.805 THz. The relative bandwidth defined as  $(f_{\max} - f_{\min})/f_0$  is as high as 179%, where  $f_{\max}$ ,  $f_{\min}$ , and  $f_0$  are the maximum, minimal, and center frequencies, respectively. As a reference, the relative bandwidth of the high coherent perfect absorption in a typical metasurface is less than 5% [15], [20]. The bandwidth of high coherent absorptivity, referring to the dispersion of the absorption spectrum, is directly derived from the dispersion of MoS<sub>2</sub>'s permittivity. It is revealed in (6) that increasing MoS<sub>2</sub> slab's thickness is, to some extent, equivalent to magnifying the effect of  $\varepsilon_{||}$ 's dispersion. Therefore, the coherent absorption spectrum becomes more dispersive and the bandwidth of high coherent absorptivity narrows. In Fig. 3(d), it is seen that when increasing the thickness of the MoS<sub>2</sub> crystal layer, the spectrum of the coherent absorptivity shifts slightly to high frequencies and its bandwidth narrows significantly. However, for the MoS<sub>2</sub> crystals with thicknesses of  $6 \mu\text{m}$  and  $7 \mu\text{m}$ , the relative bandwidths of the high coherent absorptivity ( $A_c > 90\%$ ) still keep as wide as 99.6% and 76.5%, respectively. Such a broadband high coherent absorptivity can be extensively exploited for applications in wideband absorption and THz communications.

The absorptivity in a coherent system can be controlled by adjusting the phase difference of the two input beams. Considering the forward and backward input electromagnetic fields have a phase difference  $\phi$ ,  $I_+ = I_- e^{-i\phi}$ , the total absorptivity becomes

$$A = 1 - \frac{|te^{-i\phi} + r|^2 + |t + re^{-i\phi}|^2}{2}. \quad (9)$$

In Fig. 3(d), we show the total absorptivity of a  $7 \mu\text{m}$ -thick MoS<sub>2</sub> slab as a function of phase difference  $\phi$  at the frequency of 1.52 THz. We see that the corresponding total absorptivity at this frequency can be modulated from 1.57% to 99.97% by adjusting the phase difference of the two input beams. This clearly demonstrate that coherent signals propagating through the MoS<sub>2</sub> crystal can be modulated between nearly completely blocked state to nearly completely transparent state. The modulation depth, defined as the ratio of the maximal total absorptivity to the minimal one, is as high as 63.68. This property is well suited for applications such as THz switches and modulators.

As discussed before, the electromagnetic characteristic of the MoS<sub>2</sub> crystal can be manipulated by controlling the carrier density through electrochemical doping. As a consequence, the coherent absorption performance of the MoS<sub>2</sub> crystal is highly related to the carrier density  $N$ . In Fig. 4(a), we show the coherent absorptivity spectra of MoS<sub>2</sub> crystal slabs with different carrier densities. It is seen that, when increasing the carrier density from  $2 \times 10^{17}$  to  $5 \times 10^{17} \text{ cm}^{-3}$ , the coherent absorptivity spectrum exhibits a clear blue-shift, where the frequency of the peak absorptivity shifts from 1.03 to 2.19 THz. By comparing Fig. 1(a) and Fig. 4(a), we see that at the frequencies of interest, coherent perfect absorption take place when MoS<sub>2</sub> shows metallic behavior. The resonance frequency shift is due to the fact that with the increase of carrier density, the MoS<sub>2</sub> crystal tends to exhibit more metallic behavior since its permittivity becomes more negative. However, the peak coherent absorptivity remains nearly perfect ( $A_c > 99.9\%$ ) for all the carrier densities of interest in our work. Meanwhile, the relative bandwidth of the high coherent absorptivity ( $A_c > 90\%$ ) decreases from

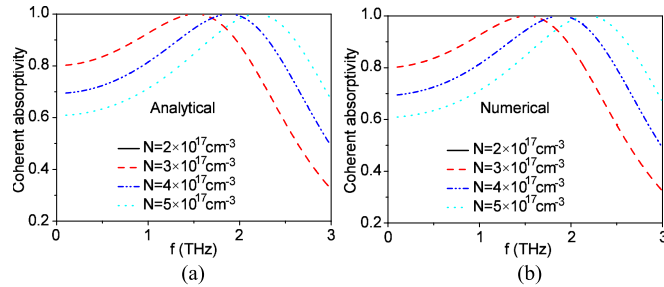


Fig. 4. (a) Analytical and (b) numerical calculation of coherent absorptivity of MoS<sub>2</sub> crystal slabs with different carrier densities. The thickness of the MoS<sub>2</sub> slab is kept at 7  $\mu\text{m}$ .

175% to 43% as the increase of carrier density. This is due to the appearance of stronger dispersion characteristics in MoS<sub>2</sub> permittivity at increased carrier densities. As a result, the spectrum of coherent absorption shows same stronger dispersion, consequently narrowing the high coherent absorptivity bandwidth.

It is worth noting that all the above calculations are based on the in-plane component of MoS<sub>2</sub> crystal's effective permittivity, which is valid when electromagnetic waves incident normally. In order to verify our analytical calculation and check whether the out-of-plane component of the effective permittivity will affect the absorption performance of the MoS<sub>2</sub> crystal, we further carry out full-wave numerical simulations using finite integration technique. In the simulations, the full anisotropic permittivity of the MoS<sub>2</sub> crystal slab is taken into consideration. As shown in Fig. 4(b), for each carrier density, the MoS<sub>2</sub> crystal slab shows exactly the same coherent absorptivity spectrum as that in Fig. 4(a), which confirms the high accuracy of our theoretical estimations.

As a final remark, we would like to note that we used a free-standing MoS<sub>2</sub> crystal merely to assist our proof of concept study and to simplify our analysis. Similar features and characteristics are also achievable using non-free-standing MoS<sub>2</sub> layers, e.g., SiO<sub>2</sub>-MoS<sub>2</sub>-SiO<sub>2</sub> sandwiched structures. It is worth mentioning that conventional semiconductors such as highly doped InSb and silicon show similar Drude type dielectric responses at terahertz frequencies. However, MoS<sub>2</sub> provides significant advantages in mechanical, electronical, and photoelectronical behaviours, and most importantly it offers the possibility to deposit layers of a few nanometers thickness, enabling many uses in highly integrated systems [26].

#### 4. Conclusion

In summary, we have theoretically demonstrated that broadband CPA can be achieved in a bulk MoS<sub>2</sub> crystal. The dispersive permittivity of bulk MoS<sub>2</sub> crystal was characterized using Drude model with parameters extracted from experiments. The reflection and transmission coefficients of an electromagnetic wave propagating through the MoS<sub>2</sub> crystal were analysed by solving the boundary conditions at the interfaces. It was shown that the electromagnetic energy of two anti-propagating waves can be almost totally absorbed by the MoS<sub>2</sub> slab and that the coherent absorptivity can be effortlessly adjusted from 1.57 to 99.97% by means of phase modulation. It was also demonstrated that the absorptivity spectrum of the MoS<sub>2</sub> crystal can be controlled by electrochemical doping. When the carrier density increases, the spectrum of coherent absorptivity exhibits a clear blueshift whilst the peak coherent absorptivity remains higher than 99.9%. To further confirm the accuracy of our theoretical estimates, we carried out full-wave numerical simulations based on finite integration technique, which shows excellent agreement with our theoretical predictions.

## References

- [1] A. K. Geim and I. V. Grigorieva, "Van der waals heterostructures," *Nature*, vol. 499, no. 7459, pp. 419–425, Jul. 2013.
- [2] Q. H. Wang, K. Kalantar-Zadeh, A. Kis, J. N. Coleman, and M. S. Strano, "Electronics and optoelectronics of two-dimensional transition metal dichalcogenides," *Nature Nanotech.*, vol. 7, no. 11, pp. 699–712, Nov. 2012.
- [3] H. RamakrishnaMatte *et al.*, "MoS<sub>2</sub> and WS<sub>2</sub> analogues of graphene," *Angew. Chem. Int. Ed.*, vol. 49, no. 24, pp. 4059–4062, Apr. 2010.
- [4] S. Sathiyan, H. Ahmad, W. Y. Chong, S. H. Lee, and S. Sivabalan, "Evolution of the polarizing effect of MoS<sub>2</sub>," *IEEE Photon. J.*, vol. 7, no. 6, Dec. 2015, Art. no. 6100610.
- [5] K. F. Mak, C. Lee, J. Hone, J. Shan, and T. F. Heinz, "Atomically thin MoS<sub>2</sub>: A new direct-gap semiconductor," *Phys. Rev. Lett.*, vol. 105, Sep. 2010, Art. no. 136805.
- [6] C. Jayasekara, M. Premaratne, S. D. Gunapala, and M. I. Stockman, "MoS<sub>2</sub> spaser," *J. Appl. Phys.*, vol. 119, no. 13, Apr. 2016, Art. no. 133101.
- [7] X.-Y. Deng, X.-H. Deng, F.-H. Su, N.-H. Liu, and J.-T. Liu, "Broadband ultra-high transmission of terahertz radiation through monolayer MoS<sub>2</sub>," *J. Appl. Phys.*, vol. 118, no. 22, Dec. 2015, Art. no. 224304.
- [8] N. I. Landy, S. Sajuyigbe, J. J. Mock, D. R. Smith, and W. J. Padilla, "Perfect metamaterial absorber," *Phys. Rev. Lett.*, vol. 100, May 2008, Art. no. 207402.
- [9] X. Liu, T. Starr, A. F. Starr, and W. J. Padilla, "Infrared spatial and frequency selective metamaterial with near-unity absorbance," *Phys. Rev. Lett.*, vol. 104, May 2010, Art. no. 207403.
- [10] W. Zhu, Y. Huang, I. D. Rukhlenko, G. Wen, and M. Premaratne, "Configurable metamaterial absorber with pseudo wideband spectrum," *Opt. Exp.*, vol. 20, no. 6, pp. 6616–6621, Mar. 2012.
- [11] Y. K. Zhong, S. M. Fu, M.-H. Tu, B.-R. Chen, and A. Lin, "A multmetal broadband metamaterial perfect absorber with compact dimension," *IEEE Photon. J.*, vol. 8, no. 2, Apr. 2016, Art. no. 6801810.
- [12] Q. Liang, T. Wang, Z. Lu, Q. Sun, Y. Fu, and W. Yu, "Metamaterial-based two dimensional plasmonic subwavelength structures offer the broadest waveband light harvesting," *Adv. Opt. Mater.*, vol. 1, no. 1, pp. 43–49, Jan. 2013.
- [13] N. Liu, M. Mesch, T. Weiss, M. Hentschel, and H. Giessen, "Infrared perfect absorber and its application as plasmonic sensor," *Nano Lett.*, vol. 10, no. 7, pp. 2342–2348, Jun. 2010.
- [14] Y. J. Yoo *et al.*, "Flexible and elastic metamaterial absorber for low frequency, based on small-size unit cell," *Appl. Phys. Lett.*, vol. 105, no. 4, Jul. 2014, Art. no. 041902.
- [15] W. Wan, Y. Chong, L. Ge, H. Noh, A. D. Stone, and H. Cao, "Time-reversed lasing and interferometric control of absorption," *Science*, vol. 331, no. 6019, pp. 889–892, Feb. 2011.
- [16] Y. D. Chong, L. Ge, H. Cao, and A. D. Stone, "Coherent perfect absorbers: Time-reversed lasers," *Phys. Rev. Lett.*, vol. 105, Jul. 2010, Art. no. 053901.
- [17] A. L. Fannin, J. W. Yoon, B. R. Wenner, J. W. Allen, M. S. Allen, and R. Magnusson, "Experimental evidence for coherent perfect absorption in guided-mode resonant silicon films," *IEEE Photon. J.*, vol. 8, no. 3, Jun. 2016, Art. no. 6802307.
- [18] J. Zhang, K. F. MacDonald, and N. I. Zheludev, "Controlling light-with-light without nonlinearity," *Light Sci. Appl.*, vol. 1, Jul. 2012, Art. no. e18.
- [19] W. Zhu, F. Xiao, M. Kang, and M. Premaratne, "Coherent perfect absorption in an all-dielectric metasurface," *Appl. Phys. Lett.*, vol. 108, no. 12, Mar. 2016, Art. no. 121901.
- [20] G. Nie, Q. Shi, Z. Zhu, and J. Shi, "Selective coherent perfect absorption in metamaterials," *Appl. Phys. Lett.*, vol. 105, no. 20, Nov. 2014, Art. no. 201909.
- [21] J. Zhang *et al.*, "Coherent perfect absorption and transparency in a nanostructured graphene film," *Opt. Exp.*, vol. 22, no. 10, pp. 12 524–12 532, May 2014.
- [22] W. Wang, X. Cui, E. Yang, Q. Fan, and B. Xiang, "Negative refraction in molybdenum disulfide," *Opt. Exp.*, vol. 23, no. 17, pp. 22 024–22 033, Aug. 2015.
- [23] A. Molina-Sánchez and L. Wirtz, "Phonons in single-layer and few-layer MoS<sub>2</sub> and WS<sub>2</sub>," *Phys. Rev. B*, vol. 84, Oct. 2011, Art. no. 155413.
- [24] X. Yan, L. Zhu, Y. Zhou, Y. E, L. Wang, and X. Xu, "Dielectric property of MoS<sub>2</sub> crystal in terahertz and visible regions," *Appl. Opt.*, vol. 54, no. 22, pp. 6732–6736, Aug. 2015.
- [25] Y. Wang, *et al.*, "Plasmon resonances of highly doped two-dimensional MoS<sub>2</sub>," *Nano Lett.*, vol. 15, no. 2, pp. 883–890, Feb. 2015.
- [26] K. F. Mak *et al.*, "Tightly bound trions in monolayer MoS<sub>2</sub>," *Nature Mater.*, vol. 12, pp. 207–211, Oct. 2013.